Orthorhombic PSDM processing, a case history in Mississippi Canyon, Gulf of Mexico

Yang He, Adam Gersztenkorn, Guy Hilburn, Sherry Yang and Bin Wang, TGS*

Summary

In areas of complex geology, especially where fractures are present, azimuthal anisotropy should be seriously considered. Tilted Transverse Isotropy (TTI), which only considers polar anisotropy, is often not sufficient for correcting moveout fluctuations detected in different azimuthal sectors. Orthorhombic anisotropy (ORT), which can describe both azimuthal and polar anisotropy, provides a more comprehensive model than the simpler Transversely Isotropic (TI) model. In this paper we present a methodology for ORT model building and imaging. The effectiveness of ORT imaging is demonstrated through its application to Orthogonal Wide Azimuth (OWAZ) data from the Gulf of Mexico (GoM). The process of ORT model building is introduced and orthorhombic tomography is applied to invert for azimuth-dependent anisotropic parameters. By resolving the inconsistencies in residual moveout for different azimuths, it is demonstrated that ORT imaging improves gather flatness in all azimuths and produces better image focusing.

Introduction

Wide azimuth (WAZ) has been established as an indispensable seismic acquisition and processing methodology for exploration and development objectives. This is especially relevant in the GoM. In comparison to a narrow azimuth survey, WAZ provides better subsurface illumination and fold coverage. TTI model building has become a standard approach for processing WAZ data in the GoM. Because TTI accounts for polar anisotropy caused by bedding and stratification, in general it improves image focusing in pre-stack depth imaging and provides flatter common image gathers (CIGs) for WAZ data.

Recently, a range of methods has been implemented to acquire data with even greater azimuthal information. Examples of this are OWAZ, (Baldock, 2011), rich azimuth (Howard, 2007), and coil shooting (Moldoveanu and Kapoor, 2009). An OWAZ survey was acquired in order to obtain a geometry that approaches full azimuth. The two orthogonal WAZ surveys, co-located in space, were acquired with nearly identical acquisition geometries. The additional azimuth and offset information from the orthogonal survey is valuable in helping to improve the accuracy of the velocity model and focusing of the final image.

While the new acquisition technologies bring rich azimuthal information that better illuminates the subsurface, they also challenge depth imaging to be able to take into account azimuthal anisotropy beyond TI. TI describes anisotropy caused by thin layering of sediments with a scale that is smaller than the predominant wavelength. The axis of symmetry is typically perpendicular to the layers and thus assumes that the velocities are the same in the transverse plane regardless of azimuth (Thomsen, 1986). Although TI takes into account velocity differences between layer planes as well as the polar direction, this may not be sufficient to describe the subsurface in areas where fractures are embedded within stratigraphic layers. In this case CIGs with different azimuths cannot be flattened with a single TTI model. There is a need within the industry for a more general model that describes azimuthal anisotropy in addition to polar anisotropy. In Figure1, synthetic data generated from ORT models with $\delta^{(1)} = 0.1$, $\delta^{(2)} = 0.05$, $\delta^{(3)} = 0.05$, $\varepsilon^{(1)} = 0.15$, $\varepsilon^{(2)} = 0.08$ are migrated with different VTI models. If the data is migrated with a VTI modelbased on the fast direction's parameters, the CIG gather for azimuth 90° is flat but the moveouts for the other five azimuths curve down. If the data is migrated with a VTI model of average δ and ε, some azimuths curve down and others curve up. ORT models can flatten all the CIGs for different azimuths (Figure 1B) as more complex but more realistic models because orthorhombic anisotropy describes seismic velocity variations in both azimuthal and polar directions.

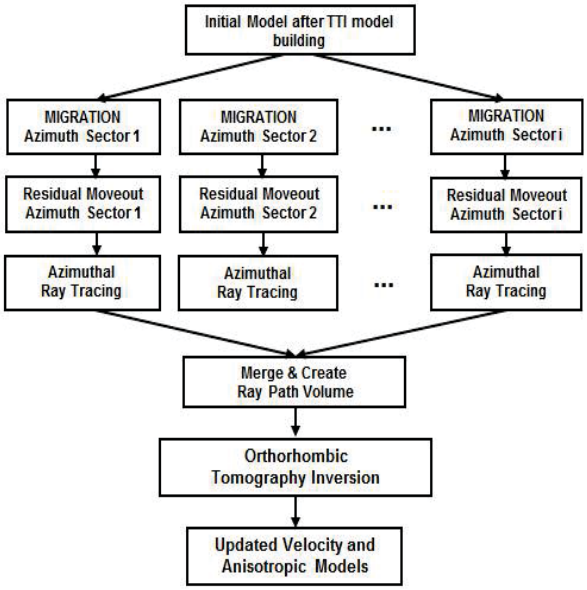

Figure 2 The workflow for orthorhombic model building.

DOI http://dx.doi.org/10.1190/segam2013-0968.1

Orthorhombic PSDM Processing

Method

The workflow for orthorhombic model building is presented in Figure 2. Initially, TTI tomography is performed to update ε_i and δ_i for each azimuth, where i refers to the i^{th} azimuth. Because each azimuth is updated individually, the gather flatness is improved with azimuth-variant ε_i and δ_i. These models of ε_i and δ_i are combined to provide initial orthorhombic parameters (Li, 2012). Although this is approximate, it is reasonable for building an initial orthorhombic model.

OWAZ data is partitioned into six azimuth sectors. These azimuth sectors are of unequal size to maintain consistent fold between sectors. Residual moveout picking and ray-tracing are performed for each azimuth sector separately. The individual ray-trace volumes (ray-paths) are combined to create a single ray-path volume which is then used to invert for a single orthorhombic model. The key for building orthorhombic models is to generate a set of $\varepsilon^{(1)}$, $\varepsilon^{(2)}$, $\delta^{(1)}$, $\delta^{(2)}$, $\delta^{(3)}$ (Tsvankin, 1997) corresponding to the local fast velocity orientation α, which can solve the inconsistency of the moveout between azimuths. Structure-oriented semblance is used for fault detection (Hale, 2009) to assist in the interpretation of faults and fractures to confirm a geologically plausible fast velocity orientation, α.

The orthorhombic phase velocity equation is as follows, (Tsvankin,1997),

$$V(\theta,\varphi) = V_0[1 + \delta(\varphi)sin^2\theta cos^2\theta + \epsilon(\varphi)sin^4\theta] \quad (1)$$

where

$$\delta(\varphi) = \delta^{(1)}sin^2\varphi + \delta^{(2)}cos^2\varphi \quad (2)$$

$$\varepsilon(\varphi) = \epsilon^{(1)}sin^4\varphi + \varepsilon^{(2)}cos^4\varphi + (2\varepsilon^{(2)} + \delta^{(3)})sin^2\varphi cos^2\varphi \quad (3)$$

It has the same form as the phase velocity in TI media, but with azimuth-dependent ε and δ. Here, θ is the polar angle and φ is the azimuthal angle. $\delta(\varphi)$ is an ellipse, while $\varepsilon(\varphi)$ is not an ellipse, with $\delta^{(3)}$ contributing to ε.

By taking the derivative of Equation (1), the sensitivity of the travel time with respect to slowness and anisotropic parameters can be obtained. Figure 3 gives the plots of the derivatives for $\theta \in$ (0, 90) and $\varphi \in$(0,360). $\frac{dt}{dS}$ is less than 1 because of anisotropic effects, while $\frac{dt}{dS} = 1$ for isotropic media. $\frac{dt}{d\delta^{(1)}}$ and $\frac{dt}{d\delta^{(2)}}$ have a perpendicular pattern, as do $\frac{dt}{d\varepsilon^{(1)}}$ and $\frac{dt}{d\varepsilon^{(2)}}$. Also, $\frac{dt}{d\delta^{(1)}}$ and $\frac{dt}{d\delta^{(2)}}$ have a value of zero at very near and far incident angles. Most non-zero values are distributed in the middle angles, while $\frac{dt}{d\varepsilon^{(1)}}$ and $\frac{dt}{d\varepsilon^{(2)}}$ are zero at near angles and have large values at far incident angles. $\frac{dt}{d\delta^{(3)}}$ is zero inside both vertical symmetric planes and has non-zero values only at far angles outside the vertical symmetric planes.

With these derivatives, the orthorhombic tomography model can be built as a linear equation system to minimize the residual moveout of gathers for all azimuths. Checkshots' travel times can be used by ray tracing in orthorhombic media as additional constraints to minimize the mis-tie.

Application

We demonstrate the ability of our method to perform multi-azimuth imaging in the presence of orthorhombic anisotropy by building ORT models for OWAZ data sets. The Kepler and Justice orthogonal WAZ surveys were acquired offshore Louisiana in the Mississippi Canyon of the GoM (Figure 4). For the study area, one large overhanging salt body dominates the survey. The salt created faults in surrounding sediment layers as it rose (Figure 5).

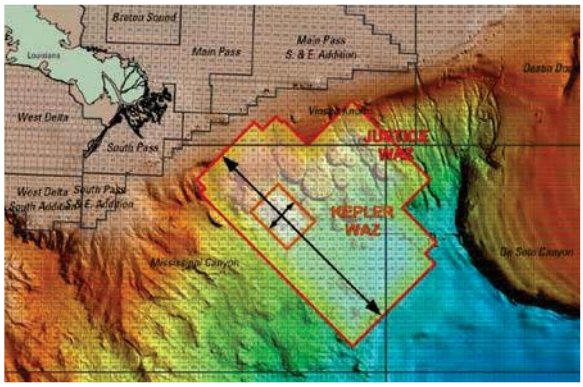

Figure 4 Map showing the orthogonal surveys.

A structure-oriented semblance algorithm detecting fault orientation (Hale, 2009) was used to produce the coherence image of the study area in Figure 5. The horizontal slice is at a depth of 6,850 meters. The seismic cross section shows a well-defined anticline that borders the salt dome approximately in the middle of the slice. The slice also shows a trend for the anticline from the upper left toward the lower right. From the slice it can be conjectured that the salt dome, which has a left-to-right orientation, rose through the surrounding sediments. The faulting, which is well-defined along the top of the anticline, follows the

DOI http://dx.doi.org/10.1190/segam2013-0968.1

trend of the anticline itself and gradually turns perpendicular to the salt body. The faulting may be due to the buckling of the anticline, with possible fractures aligned parallel to the faults themselves. The complex geology caused uneven stress and azimuthal anisotropy.

In the final stage of TTI model building using OWAZ data,v_0, ε_0, δ_0, θ, and φ are used for an initial model for ORT imaging. Moveout discrepancy on CIGs from different azimuths is observed in some locations (Figure 7). This could be due to the inability of simple TTI models to realistically describe the true anisotropy. The presence of orthorhombic anisotropy poses challenges in OWAZ imaging. With orthorhombic model building and migration, the image focusing is improved in the deep section, and the reflector underneath the carbonate zone has less fluctuation. This indicates simpler geologic structures (Figure 6) with the overburden models solving the conflicting moveout among azimuths (Figure 7).

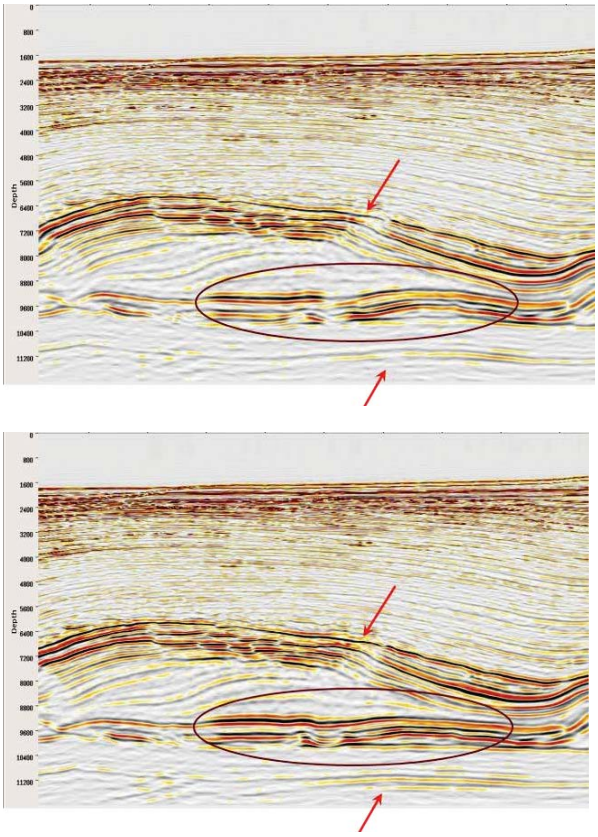

Figure 6 The stacking images for the study area. The upper one is the stacking image from the TTI final migration. The lower one is from the orthorhombic migration.

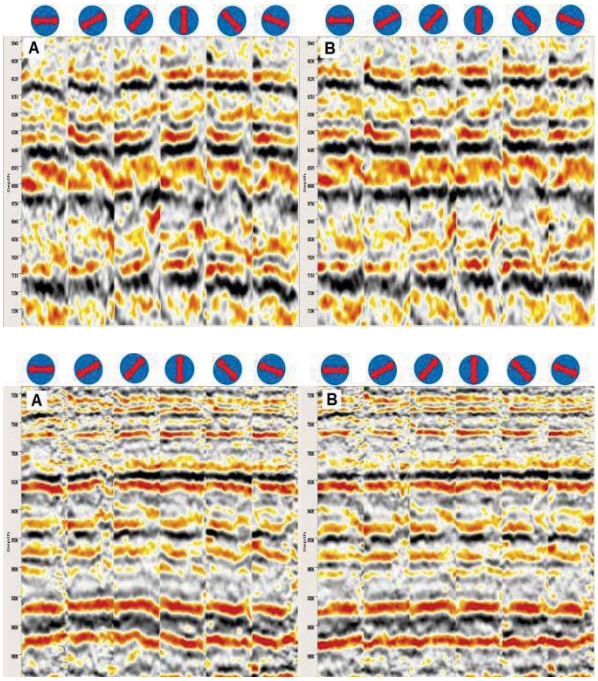

Figure 7 Comparison of two different CIG locations for six azimuth angles extracted from the study area. A) The gathers from the final TTI migration. Inconsistency in the residual moveouts is observed between different azimuths. B) The gathers from orthorhombic migration. Gather flatness is improved for all azimuths. Azimuths range from 0 to 150° with an interval of 30°.

Conclusions

We have introduced the process of orthorhombic model building and investigated the derivatives for orthorhombic tomography. By using our orthorhombic PSDM approach, we managed to account for anisotropy in both azimuthal and polar directions for the Kepler and Justice orthogonal WAZ data. Rich azimuthal information is utilized to derive an ORT model. Orthorhombic anisotropic PSDM reduced the structural discrepancies between seismic images built for different azimuths, produced a constructive summation of OWAZ datasets, and provided significant imaging uplift.

Acknowledgements

Authors would like to thank Zhiming Li, Laurie Geiger and Chuck Mason for reviewing the paper. We thank TGS management for permission to publish this paper.

DOI http://dx.doi.org/10.1190/segam2013-0968.1

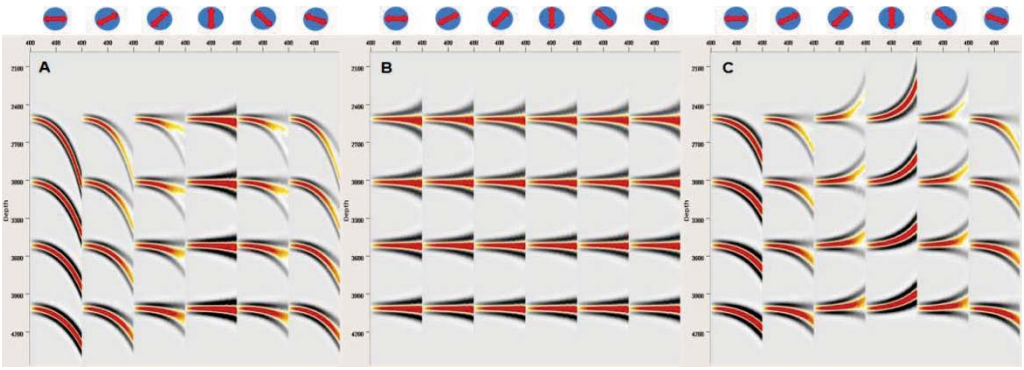

Figure 1 Migration gathers for 6 azimuth angles (0, 30˚, 60˚, 90˚, 120˚,150˚). A) VTI migration gathers with $\delta = 0.1, \varepsilon = 0.15$. B) Orthorhombic migration gathers with $\delta^{(1)} = 0.1$, $\delta^{(2)} = 0.05$, $\delta^{(3)} = 0.05$, $\varepsilon^{(1)} = 0.15$, $\varepsilon^{(2)} = 0.08$. C) VTI migration gathers with $\delta = 0.075$, $\varepsilon = 0.115$.

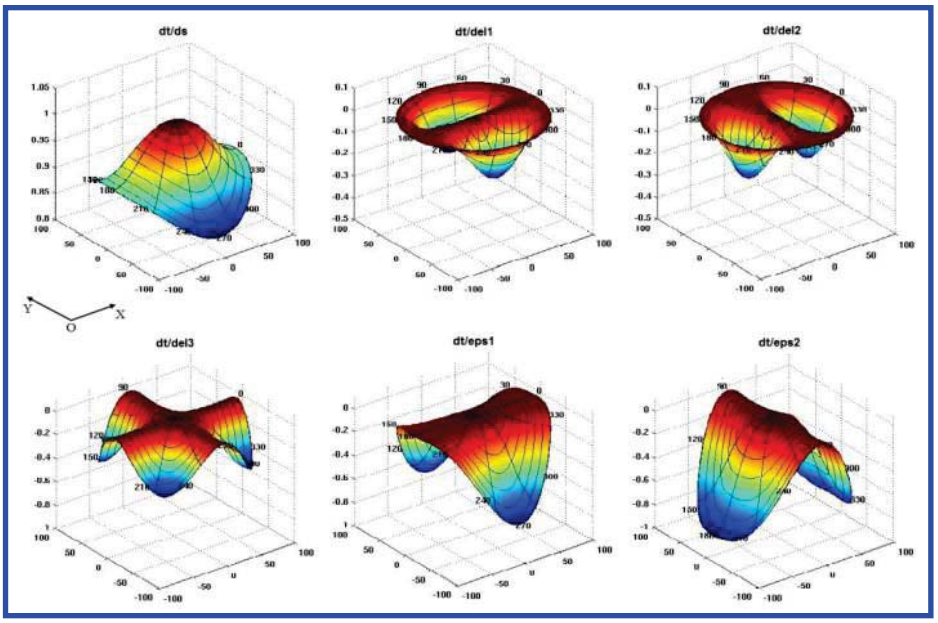

Figure 3 The derivatives of orthorhombic parameters for $\varepsilon^{(1)}$=0.2, $\varepsilon^{(2)}$=0.1, $\delta^{(1)}$=0.12, $\delta^{(2)}$=0.06, $\delta^{(3)}$=0.05. The vertical axis represents the value of the derivatives. Azimuths are plotted from 0 to 360˚ with an interval of 30˚.Polar angles are plotted from 0 to 90˚.

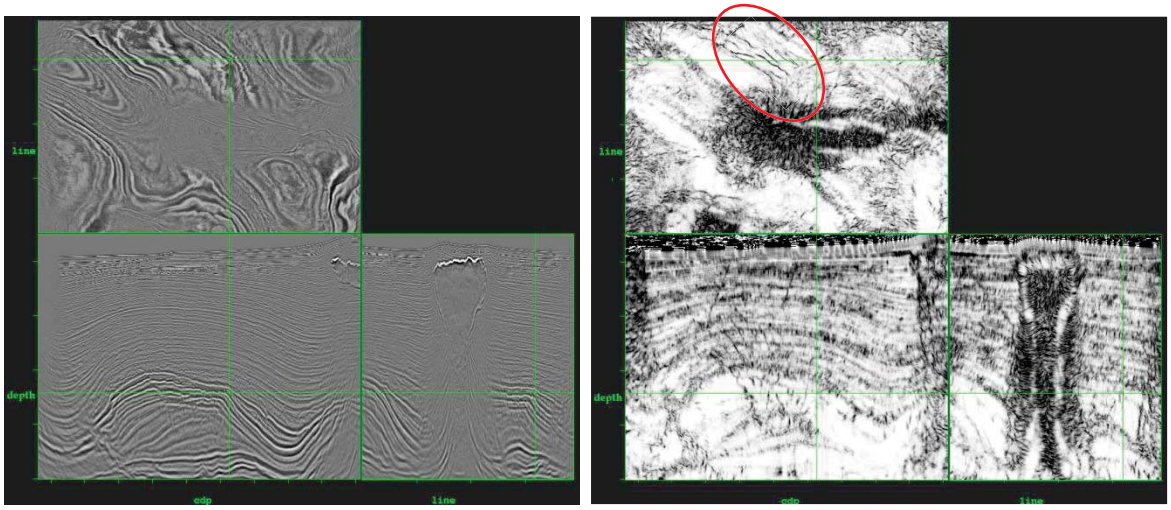

Figure 5 On the left is the seismic image in the study area, with a large salt body in the middle. On the right is the coherence figure showing fault orientation. Faults are parallel to the trend of the anticline and go perpendicular to the salt boundary.

DOI http://dx.doi.org/10.1190/segam2013-0968.1

http://dx.doi.org/10.1190/segam2013-0968.1

EDITED REFERENCES

Note: This reference list is a copy-edited version of the reference list submitted by the author. Reference lists for the 2013 SEG Technical Program Expanded Abstracts have been copy edited so that references provided with the online metadata for each paper will achieve a high degree of linking to cited sources that appear on the Web.

REFERENCES

Baldock, S., C. Reta-Tang, B. Beck, W. Gao, E. Doue and S. Hightower, 2011, Orthogonal wide azimuth surveys: Acquisition and Imaging: 81st Annual International Meeting, SEG, Expanded Abstracts, 147–151.

Hale, D., 2009, Structure-oriented smoothing and semblance: CWP Report 635.

Howard, M., 2007, Marine seismic surveys with enhanced azimuth coverage: Lessons in survey design and acquisition: The Leading Edge, **26**, 480–493.

Li, Y., W. Han, C. Chen, and T. Huang, 2012, Velocity model building for tilted orthorhombic depth imaging: 82nd Annual International Meeting, SEG, Expanded Abstracts, 1–5.

Moldoveanu, N., and J. Kapoor, 2009, What is the next step after WAZ for exploration in the Gulf of Mexico?: 79th Annual International Meeting, SEG, Expanded Abstracts, **28**, 41.

Thomsen, L., 1986, Weak elastic anisotropy: Geophysics, **51**, 1954–1996.

Tsvankin, I., 1997, Anisotropic parameters and P-wave velocity for orthorhombic media: Geophysics, **62**, 1292–1309.